

# Spin texture and its impact on superconductivity in underdoped cuprates: a $\mu$ SR investigation of $(\text{Ca}_x\text{La}_{1-x})(\text{Ba}_{1.75-x}\text{La}_{0.25+x})\text{Cu}_3\text{O}_y$

<sup>1</sup>Amit Kanigel, <sup>1</sup>Amit Keren, <sup>1</sup>Yaakov Eckstein, <sup>1</sup>Arkady Knizhnik, <sup>2</sup>James S. Lord, and <sup>3</sup>Alex Amato

<sup>1</sup>Physics Department, Technion-Israel Institute of Technology, Haifa 32000, Israel.

<sup>2</sup>Rutherford Appleton Laboratory, Chilton Didcot, Oxfordshire OX11 0QX, U.K.

<sup>3</sup>Paul Scherrer Institute, CH 5232 Villigen PSI, Switzerland  
(December 2, 2024)

We characterize the spontaneous magnetic field, and determine the associated temperature  $T_g$ , in the superconducting state of  $(\text{Ca}_x\text{La}_{1-x})(\text{Ba}_{1.75-x}\text{La}_{0.25+x})\text{Cu}_3\text{O}_y$  using zero and longitudinal field  $\mu$ SR measurements for various values of  $x$  and  $y$ . Our major findings are: (I) the higher  $T_g$  is in the underdoped region, the higher the  $T_c$  is in the optimally doped sample, (II) the phase separation between hole poor and hole rich regions is a *microscopic* one, and (III) spontaneous magnetic fields appear gradually with no moment size evolution.

There is growing evidence that at low temperatures, cuprates phase-separate into regions that are hole “poor” and hole “rich”<sup>1</sup>. While hole rich regions become superconducting below  $T_c$ , the behavior of hole poor regions at these temperatures is not quite clear. Some data support the existence of magnetic moments in these regions. In impure cases, like Zn or Li doped YBCO, the impurity creates both the hole poor regions<sup>2</sup> and the magnetic moments<sup>3,4</sup>. In pure cases, such as LSCO, these magnetic moments are created spontaneously and undergo a spin glass like freezing at  $T_g$ <sup>5</sup>. However, there are still many open questions regarding these moments and the spontaneous magnetic fields associated with them. For example: Is there a true phase transition at  $T_g$ ? What is the field profile and how is it different from, or similar to, a canonical spin glass? Is the field confined solely to the hole poor regions or does it penetrate the hole rich regions? Also, the interplay between magnetism and superconductivity is not clear. Is strong magnetic background beneficial or detrimental to superconductivity?

We address these questions by performing zero and longitudinal field muon spin relaxation experiments on a series of polycrystalline  $(\text{Ca}_x\text{La}_{1-x})(\text{Ba}_{1.75-x}\text{La}_{0.25+x})\text{Cu}_3\text{O}_y$  (CLBLCO) samples. This superconductor belongs to the 1:2:3 family and has several properties that make it ideal for our purpose. It is tetragonal throughout its range of existence  $0 \leq x \lesssim 0.5$ , so there is no ordering of CuO chains. Simple valence sums<sup>6</sup>, more sophisticated bond-valance calculations<sup>7</sup>, and thermoelectric power measurements<sup>8</sup> show that the hole concentration is  $x$  independent. As shown in Fig. 1, by changing  $y$ , for a constant value of  $x$ , the full superconductivity curve, from the under-doped to the over-doped, can be obtained. Finally, for different Ca contents, parallel curves of  $T_c$  vs  $y$  are generated. Therefore, with CLBLCO one can move continuously, and with minimal structural changes, from a superconductor resembling YBCO to one similar to LSCO.

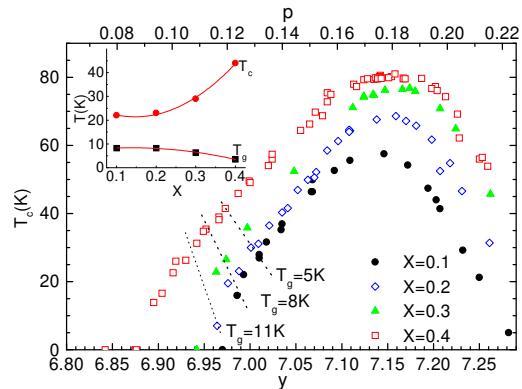


FIG. 1. Phase digram of  $(\text{Ca}_x\text{La}_{1-x})(\text{Ba}_{1.75-x}\text{La}_{0.25+x})\text{Cu}_3\text{O}_y$ .  $p$  is the hole density per plane<sup>6</sup>. The dashed lines indicate samples with equal  $T_g$  values as shown. Inset:  $T_c$  and  $T_g$  versus  $x$  for  $y = 6.98$ .

The preparation of the samples is described elsewhere<sup>9</sup>. Oxygen content was determined using iodometric titration. All the samples were characterized using X-ray diffraction and were found to be single phase.  $T_c$  is obtained from resistivity measurements. We also verified that CLBLCO respects the Uemura relations<sup>10</sup>.

The  $\mu$ SR experiments were done at two facilities. When a good determination of the base line was needed we used the ISIS pulsed muon facility, Rutherford Appleton Laboratory, UK. When high timing resolution was required we worked at Paul Scherrer Institute, Switzerland (PSI). Most of the data were taken with a <sup>4</sup>He cryostat. However, in order to study the internal field profile we had to avoid dynamical fluctuations by freezing the moments completely. For this purpose we used the <sup>3</sup>He cryostat at ISIS with a base temperature of 350 mK.

Typical muon asymmetry  $[A(t)]$  depolarization curves, proportional to the muon polarization  $P_z(t)$ , are shown in Fig. 2 (a) for different temperatures in the  $x = 0.1$  and  $y = 7.012$  ( $T_c = 33.1\text{K}$ ) sample. The change of the

polarization shape with temperature indicates a freezing process, and the data can be divided into three temperature regions. In region (I), given by  $T \gtrsim 8$ , the muon relaxes according to the well known Kubo-Toyabe (KT) function, typical of the case where only frozen nuclear moments are present<sup>11</sup>. In region (II), bounded by  $8 \gtrsim T \gtrsim 3$ , part of the polarization relaxes fast and the rest as in the first region. As the temperature is lowered the fast portion increases at the expense of the slow one. Moreover, the relaxation rate in the fast portion seems independent of temperature. Finally, at long time the asymmetry relaxes to zero. In region (III), where  $3 \gtrsim T$ , the asymmetry at long times no longer relaxes to zero, but instead recovers to a finite value. This value is  $\sim 1/3$  of the initial asymmetry  $A_z(0)$ .

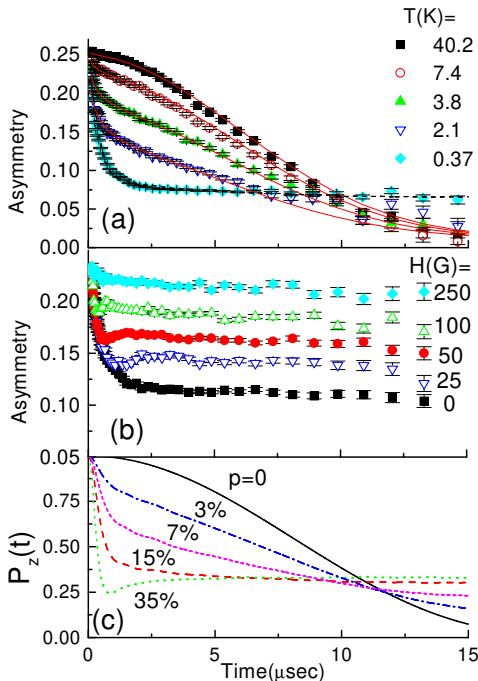


FIG. 2. (a) ZF- $\mu$ SR spectra obtained in a  $x = 0.1$ ,  $y = 7.012$  sample. The solid lines are fit to the data using Eq. 1, the dashed line is a fit using the simulation as described in the text. (b)  $\mu$ SR spectra obtained in longitudinal fields from the  $x = 0.4$ ,  $y = 6.984$  sample at 350mK. (c) Polarization curves generated by the simulation program as described in the text.

To demonstrate that the internal field is static at base temperature, the muon polarization was measured with an external field applied parallel to the initial muon spin-polarization. This geometry allows one to distinguish between dynamic and static internal fields. In the dynamic case the asymmetry is field independent<sup>12</sup>. In contrast, in the static case the total field experienced by the muon is a vector sum of  $H$  and the internal fields, which are of order  $\langle B^2 \rangle^{1/2}$ . For  $H \gg \langle B^2 \rangle^{1/2}$  the total field is nearly parallel to the polarization. Therefore, in the static case, as  $H$  increases, the depolarization decreases, and the asymme-

try recovers to its initial value. Because we are dealing with a superconductor this field sweep was done in field-cool conditions. Every time the field was changed the sample was warmed up above  $T_c$  and cooled down in a new field. The results are shown in Fig. 2(b). At an external field of 250 G, the total asymmetry is nearly recovered. This indicates that the internal field is static and of the order of tens of Gauss.

We divide the data analysis into two parts: high temperatures (region II), and base temperature. First we discuss region II. Here we focus on the determination of  $T_g$ . For that purpose we fit a combination of a fast relaxing function and a KT function to the data

$$A_z(t) = A_m \exp(-\sqrt{\lambda t}) + A_n \text{KT}(t), \quad (1)$$

where  $A_m$  denotes the amplitude of the magnetic part,  $\lambda$  is the relaxation rate of the magnetic part, and  $A_n$  is the amplitude of the nuclear part. The relaxation rate of the KT part was determined at high temperatures and is assumed to be temperature independent. The sum  $A_m + A_n$  is constrained to be equal to the total initial asymmetry at high temperatures. In the first fitting round, the parameter  $\lambda$  was found to be temperature independent (as pointed out above). Therefore, it is taken as a global parameter in the final analysis. The solid lines in Fig. 2 are the fits to the data using Eq. 1.

The success of this fit indicates the simultaneous presence of two phases in the sample; part of the muons probe the magnetic phase while others probe only nuclear moments. As the temperature decreases  $A_m$ , which is presented in the insert of Fig. 3, grows at the expense of  $A_n$ . The origin of the magnetic phase is electronic moments that slow down and freeze in a random orientation. The fact that  $\lambda$  is temperature independent means that in the magnetic phase  $\gamma_\mu \langle B^2 \rangle^{1/2}$ , where  $\gamma_\mu$  is the muon gyromagnetic ratio, is temperature independent. In other words, as the temperature is lowered, more and more parts of the sample become magnetic, but the moments in these parts saturate upon freezing. At low enough temperature  $A_m$  saturates.

Our criterion for  $T_g$  is the temperature at which  $A_m$  is half of the total muon polarization as demonstrated by the vertical line in the insert of Fig. 3. The phase diagram that is shown in Fig. 3 represents  $T_g$  for various samples differing in Ca and O contents. This diagram is systematic and rather smooth suggesting good control of sample preparation. As expected, for constant  $x$ , higher doping gives lower  $T_g$ .

We have singled out three groups of samples with a common  $T_g = 11, 8$  and  $5$  K as shown in Fig. 3 by the horizontal solid lines. These samples are represented in the phase diagram in Fig. 1 by the dotted lines. The phase diagram, containing both  $T_g$  and  $T_c$ , is the first main finding of this work. It provides clear evidence of the important role of the magnetic phase in high temperature superconductivity. Let us consider samples with the same  $T_c$  (*e.g.* along a horizontal line). It is known

from the Uemura relation that  $T_c \propto n_s$  where  $n_s$  is the superconducting carrier density (assuming identical carrier mass  $m^*$ )<sup>13,10</sup>. If we now increase the oxygen content of these samples, then those that have started off with higher  $T_g$  will reach higher maximum  $T_c$  at optimal doping. In other words, doping against a strong magnetic background is helpful for high  $T_c$ .

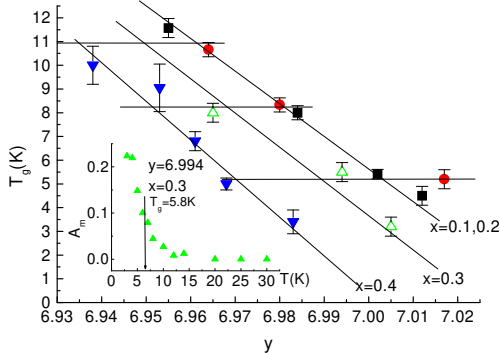


FIG. 3.  $T_g$  vs.  $y$ . The horizontal solid lines are the equal  $T_g$  lines appearing in Fig 1. Inset: Magnetic amplitude as function of temperature for a  $x = 0.3$   $y = 6.994$  sample. The arrow indicates  $T_g$  of that sample.

Another interesting aspect is the dependence of  $T_g$  and  $T_c$  on  $x$  for constant  $y$ , namely, constant doping. In the inset of Fig. 1 we show  $T_g$  and  $T_c$  for samples with  $y = 6.98$ . The dependence of both these temperatures on the Ca content is not linear. At low Ca levels  $T_g$  is almost  $x$  independent, but as  $x$  increases  $T_g$  decreases. A similar but opposite behavior occurs with  $T_c$ . This points to a correlation between the magnetic and superconducting transition temperatures, for a given doping level.

We now turn to discuss the muon depolarization at base temperature. In this case all the muons experience only a static magnetic field, as proven above. This allows one to reconstruct the internal field distribution out of the polarization curve. The polarization of a muon spin experiencing a unique field  $\mathbf{B}$  is given by  $P_z(t) = \cos^2(\theta) + \sin^2(\theta) \cos(\gamma|\mathbf{B}|t)$ , where  $\theta$  is the angle between the field and the initial spin direction. When there is an isotropic distribution of fields, a 3D powder averaging leads to

$$P_z(t) = \frac{1}{3} + \frac{2}{3} \int_0^\infty \rho(|B|) \cos(\gamma|B|t) B^2 dB \quad (2)$$

where  $\rho(|B|)$  is the distribution of  $|\mathbf{B}|$ . Therefore, the polarization is given by the Fourier transform of  $\rho(|B|)B^2$  and has a 1/3 base line. When the distribution of  $\mathbf{B}$  is centered around zero field,  $\rho(|B|)B^2$  is a function with a peak at  $\langle B \rangle$  and a width  $\Delta$ , and both these numbers are of the same order of magnitude [e.g. Fig 4(b)]. Therefore we expect the polarization to have a damped oscillation and to recover to 1/3, a phenomenon known as the dip [e.g. the inset in Fig 4 (b)]. Gaussian, Lorentzian and even exponential random field distribution<sup>14</sup>, and, more

importantly, all known canonical spin glasses, produce polarization curves that have a dip before the 1/3 recovery. Therefore, the most outstanding feature of the muon polarization curve at base temperature is the fact that no dip is present, although there is a 1/3 tail. This behavior was found in all of our samples with  $T_c > 7$  K, and also in Ca doped YBCO<sup>15</sup> and Li doped YBCO<sup>16</sup>.

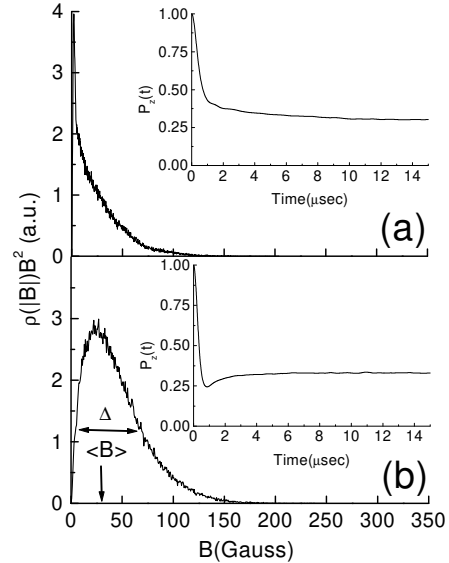


FIG. 4. (a) The internal field distribution extracted from the simulations for the case of correlation length  $\xi = 3$  lattice constants, maximum moment size of  $0.06\mu_B$  and magnetic moment concentration  $p = 15\%$ . Inset: The muon spin polarization for that distribution. (b) The same as above for the case of  $p=35\%$ .

The lack of the dip in  $P_z(t)$  can tell much about the internal field distribution. It means that  $\langle B \rangle$  is much smaller than  $\Delta$ . In that case the oscillations will be over-damped and the polarization dipless! In Fig. 4 we show, in addition to the  $\langle B \rangle \simeq \Delta$  [panel (b)] case described above, a field distribution that peaks around zero [panel (a)]. Here  $\langle B \rangle$  is smaller than  $\Delta$ , and, indeed, the associated polarization in the inset is dipless. Thus in order to fit the base temperature polarization curve we should look for  $\rho(|B|)B^2$  with most of its weight around zero field. This means that  $\rho(|B|)$  diverges like  $1/B^2$  at  $|B| \rightarrow 0$ , namely, there is abnormally high number of lower field sites.

The 1/3 recovery is also very significant. It means that the phase separation is not a macroscopic one. If it were, all muons in the field free part would have  $P_z(t) = 1$  at all times, and all muons in the magnetic part would have  $\lim_{t \rightarrow \infty} P_z(t) = 1/3$ . The total would be higher than 1/3, in contrast to observation. Thus, the superconducting and magnetic regions are intercalated on a microscopic

scale ( $\sim 20\text{\AA}$ )<sup>17</sup>. This is the second main finding of this work.

The special internal field distribution, and the nature of the gradual freezing of the spins, can be explained by the intrinsic inhomogeneity of hole concentration. The part of the sample that is hole poor, and for that reason is “more” antiferromagnetic, will freeze, while the part which is hole rich will not freeze at all. The variation in the freezing temperature of different parts of the sample can be explained by the distribution of sizes and hole concentration in these antiferromagnetic islands<sup>18</sup>. The large number of low field sites is a result of the fact that the magnetic field generated in the magnetic regions will penetrate into the hole rich regions but not completely.

To improve our understanding of the muon polarization, we performed simulations of a toy model aimed at reproducing the results described above. A 2D  $100 \times 100$  square lattice is filled with two kinds of moments, nuclear and electronic. All the nuclear moments are of the same size, they are frozen and they point in random directions. Out of the electronic moments only a small fraction  $p$  is assumed to be frozen; they represent magnetic regions with uncompensated antiferromagnetic interactions. Since these regions may vary in size the moments representing them are random, up to a maximum size. The frozen electronic moments induce spin polarization in the other electronic moments surrounding them. Following the work of others<sup>19</sup>, we use decaying staggered spin susceptibility which we take to be exponential, namely,

$$\chi'(\mathbf{r}) = (-1)^{n_x+n_y} \exp(-r/\xi) \quad (3)$$

where  $\mathbf{r} = n_x a \hat{x} + n_y a \hat{y}$  represents the position of the neighbor Cu sites,  $\mathbf{a}$  is the lattice vector, and  $\xi$  is the characteristic length scale. Because of this decay, at low frozen spin concentration, large parts of the lattice are practically field free (expect for nuclear moments). However, the important point is that no clear distinction between magnetic and field free (superconducting) regions exists.

The muon polarization time evolution in this kind of field distribution is numerically simulated. The interaction between the muon and all the other moments is taken to be dipolar, and  $\xi$  is taken to be 3 lattice constants<sup>1,2</sup>. The dashed line in Fig. 2 is a fit to the  $T = 350$  mK data, which yield  $p = 15\%$  and maximum moment size  $\simeq 0.06\mu_B$ . As can be seen, the line fits the data very well. However, as expected, the fit is sensitive to  $\sqrt{p}\xi$  only, so longer  $\xi$  would have given smaller  $p$ . The field distributions and the polarization curve shown in Fig. 4 were actually generated using the simulation. In (a) the spin density is 15% while in (b) the density is 35%.

In panel (c) of Fig. 2 we show the spin polarization for different hole concentration, varying from 0% to 35%. The resemblance between the simulation results and the muon polarization as a function of temperature in panel (a) leads us to our third conclusion that the freezing pro-

cess is mostly a growth in the number of frozen AF islands.

We are now in a position to address the questions presented in the introduction. The appearance of spontaneous magnetic field in CLBLCO is a gradual process. As the temperature is lowered microscopic regions of frozen moments appear in the samples, and their number increases but the moments do not. In the ground state the field profile is very different from that of a canonical spin glass or any other standard magnet. It could only be generated by microscopic intercalation of an abnormal number of zero field regions with magnetic regions without a clear distinction between the two. Finally, the relation between maximum  $T_c$  and  $T_g$  leads us to believe that the presence of strong magnetic interactions at low doping is important for high temperature superconductivity at optimal doping.

We would like to thank the PSI and ISIS facilities for their kind hospitality and continuing support of this project, This work was funded by the Israeli Science Foundation, the EU-TMR program, and the Technion V. P. R fund - Posnansky, and P. and E. Nathen, research funds.

- 
- <sup>1</sup> C. Howald *et al.*, cond-mat/0101251, J.M. Tranquada *et al.*, Nature **375**, 561 (1995); V.J. Emery and S.A. Kivelson, Physica C **209**, 597 (1993).
- <sup>2</sup> B. Nachumi *et al.* Phys. Rev. Lett. **77**, 5421 (1996); S. H. Pan *et al.*, Nature **401**, 746 (2000).
- <sup>3</sup> P. Mendels *et al.*, Phys. Rev. B **49**, 10035 (1994).
- <sup>4</sup> J. Bobroff *et al.*, Phys. Rev. Lett. **86**, 4116 (2001).
- <sup>5</sup> C. Niedermayer *et al.* Phys. Rev. Lett. **80**, 3843 (1998); F. C. Chou *et al.*, Phys. Rev. Lett. **71**, 2323 (1993).
- <sup>6</sup> The density of hole per plane is  $p = -0.205 + y/3$ .
- <sup>7</sup> O. Chmaissem *et al.*, Phys. Rev. B **63**, 174510 (2001).
- <sup>8</sup> A. Knizhnik *et al.*, Physica C **321**, 199 (1999).
- <sup>9</sup> D. Goldschmidt *et al.*, Phys. Rev. B **48**, 532 (1993).
- <sup>10</sup> To be published.
- <sup>11</sup> *Muon Science: Muons in Physics, Chemistry and Materials*, Eds S. L. Lee, S. H. Kilcoyne and R. Cywinski (Institute of Physics, London), 1999.
- <sup>12</sup> As long as  $\gamma_\mu H < \nu$ , where  $\nu$  is the fluctuation rate.
- <sup>13</sup> Y. J. Uemura *et al.*, Phys. Rev. Lett. **62**, 2317 (1989).
- <sup>14</sup> M. I. Larkin *et al.*, Phys. Rev. Lett. **85**, 1982 (2000).
- <sup>15</sup> C. Bernhard *et al.* Phys. Rev. B **58**, 8937 (1998).
- <sup>16</sup> P. Mendels (private communication).
- <sup>17</sup> A moment of  $1\mu_B$  will induce a 1G field at a distance of  $\sim 20\text{\AA}$ . This field is equivalent to the nuclear moments background.
- <sup>18</sup> J.H. Cho *et al.*, Phys. Rev. B **46**, 3179 (1992).
- <sup>19</sup> A. J. Millis, H. Monien, and D. Pines, Phys. Rev. B **42**, 167 (1990); J. Bobroff *et al.*, Phys. Rev. Lett. **79**, 2117 (1997); M. H. Julien *et al.*, Phys. Rev. Lett. **84**, 3422 (2000).